*Int. J. Electrochem. Sci.*, 11 **(2016)** 2401 - 2407

International Journal of
ELECTROCHEMICAL
SCIENCE
www.electrochemsci.org

# Employment of $TiO_2$/AC as Particulate Electrode for Efficient Phenol Oxidation

*Wang Lizhang*[1,*], *Zhao Yu*[2], *Yang Shengxiang*[1], *Wu Bo*[1], *Li Peng*[3], *Zhao Yuemin*[4]

[1]School of Environment Science and Spatial Informatics, China University of Mining and Technology, Xuzhou City, Jiangsu, 221116, P. R. China.
[2]Chimey Environment Science and Technology Company, Hangzhou City, Zhejiang, 310030, P. R. China.
[3]School of Water Resource & Environmental Engineering, East China Institute of Technology, Nanchang City, Jiangxi, 330013, P. R. China.
[4]School of Chemical Engineering and Technology, China University of Mining and Technology, Xuzhou City, Jiangsu, 221116, P. R. China
[*]E-mail: wlzh0731@126.com

*Received:* 8 December 2015 / *Accepted:* 25 December 2015 / *Published:* 1 February 2016

Titanium dioxide ($TiO_2$) doped activated carbon ($TiO_2$/AC) was prepared and its morphology, microstructure and phase composition were characterized by transmission electron microscope (TEM), X-ray diffraction (XRD) and X-ray photoelectron spectroscopy (XPS) tests. Cyclic voltammetry (CV) and electrochemical impedance spectroscopy (EIS) measurements were used to investigate electrochemical properties of the $TiO_2$/AC. The results revealed nano-$TiO_2$ in monocrystal state could uniformly disperse into AC, the feed current and exchange current density obtained in CV results and EIS analysis all were obviously enhanced, indicating $TiO_2$ exhibited its electrocatalytic activity by employment as an insulator to enhance bipolarity of AC particles. As a result, the excellent electrochemical performances of $TiO_2$/AC brought about the increase of space-time yield and decrease of power consumption for phenol oxidation. Further, the $TiO_2$/AC electrode could reduce intermediate generation by shortening phenol degradation pathway.

**Keywords:** $TiO_2$ doped activated carbon ($TiO_2$/AC); phenol; electrooxidation; electro-catalyst

## 1. INTRODUCTION

The performance of a packed-bed electrode is superior to merely anodic oxidation for the electrode area expansion of bipolar particles in a high gradient electric field [1-3]. Aiming to further increase space-time yield (STY), metal oxide (ZnO, $MnO_x$ or $SnO_2$) doped on activated carbon (AC) or

others particles was frequently used as particulate electrode [4-6]. As another low cost and easy nano-dispersion catalyst, titanium dioxide ($TiO_2$) was introduced into synthesis of $TiO_2$ doped active carbon ($TiO_2$/AC) and the reconstructed particles exhibits attractive catalytic ability in photoexcited generation of hydroxyl radicals [7,8]. Although numerous literatures reported $TiO_2$ could be electrically induced [9,10], we also proposed a model to describe electrooxidation and confirmed the enhancement of the STY was for the increase of the contact resistance between $TiO_2$/AC particles [11]. However, the quantitatively electrochemical performances and oxidation pathway for organic compounds in an electric field remains unclear. Consequently, it is very necessary to further investigate intrinsic roles of $TiO_2$ played in electrolysis.

In this study, sol-gel method was employed for $TiO_2$/AC preparation and its phase composition and structural analysis were characterized through transmission electron microscope (TEM), X-ray diffraction (XRD) and X-ray photoelectron spectroscopy (XPS) tests. Cyclic voltammetry (CV) and electrochemical impedance spectroscopy (EIS) measurements were conducted to evaluate the electrochemical properties of AC and $TiO_2$/AC electrodes. Then, phenol oxidation on the two electrodes was performed and the degradation pathways were determined by ultraviolet (UV) and gas chromatography-mass spectrometry (GC-MS) analysis.

## 2. EXPERIMENTAL SECTION

During sol-gel prepared the $TiO_2$/AC, the sol was synthesized from anhydrous ethanol ($C_2H_6O$), glacial acetic acid ($C_2H_4O_2$) and tetrabutyl titanate ($C_{16}H_{36}O_4Ti$) with volume ratio of 2.8:1:1, and mixed by $C_2H_6O$ aqueous solution (volume ratio of 1:1). Then, oven-dried AC with an average particle size of 5.0 mm was introduced into the hybrid and stirred for about 30 minutes. The samples aged for 2 to 3 days was firstly dried at 105 ºC for 7 h and subsequently baked at 550 ºC under nitrogen protection for 2.5 h.

The morphologies of AC and $TiO_2$/AC were obtained using TEM with type of Tecnai G2F20 and a Bruker instrument with $Cu_{K\alpha}$ radiation was used for XRD pattern test. The phase composition was measured by an XPS (model: ESCALAB 250Xi) and an ASAP 2460 system was used to analyze porosities of AC and $TiO_2$/AC by nitrogen adsorption at 77 K. CV and EIS measurements were carried out in phenolic solution (phenol 600 mg/L, $Na_2SO_4$ 3% *w*/*w*) using a three electrode cell coupled to a CS310 electrochemical workstation (Wuhan Corrtest Company). Ti plate (5×4 cm) was chosen as counter electrode, and composite electrode consisted of $IrO_2$-$Ta_2O_5$/Ti anode with size of 5×4 cm and activate mass ($TiO_2$/AC or AC) was used as working electrode.

Phenol oxidation was performed in a process composed of eight units with 10×5×15 cm dimension by packing AC or $TiO_2$/AC into electrode gaps under continuous flow mode, $IrO_2$-$Ta_2O_5$/Ti and Ti plates (10×10 cm) were employed as anode and cathode, respectively, and the experimental details were shown elsewhere [12]. UV absorption spectra of samples were measured by a Specord 200 UV-vis spectrophotometer and the intermediates generated during phenol oxidation were identified by GC-MS analyser with model Agilent 7890-5975C. The chemical oxygen demand (COD)

content determined by standard method [13] was employed to calculate the values of STY and power consumption $E_{sp}$.

$$\mathrm{STY} = \frac{q(\mathrm{COD}_0 - \mathrm{COD}_t)}{V_e(t)} \quad (1)$$

$$E_{sp} = \frac{UI}{q(\mathrm{COD}_0 - \mathrm{COD}_t)} \quad (2)$$

where $V_e(t)$ is the effective electrolyte volume at reaction time $t$, $U$ the applied voltage, $I$ the applied current, $q$ the flow rate, $\mathrm{COD}_0$ and $\mathrm{COD}_t$ the COD values at reaction time 0 and $t$.

## 3. RESULTS AND DISCUSSION

Fig. 1 shows the microstructure and component of AC and the prepared $TiO_2$/AC. The strong diffraction peaks of XRD pattern of the sample shown in Fig. 1(a) can be evidently indexed to anatase $TiO_2$ (JCPDS no. 21-1272), which demonstrates the good organization of $TiO_2$ and AC. No obvious diffraction peak associated with carbon is observed, suggesting AC in the $TiO_2$/AC is disordered. Calculated from Scherrer's formula, the average size of synthesized $TiO_2$ particles is estimated as 16.8 nm with half peak width of lattice plane (101), which is accordance to TEM result described by Fig. 1(b). We can see from Fig. 1(c) the microporous of fresh AC are fairly scarce, which would maybe decrease quantity of the active spot.

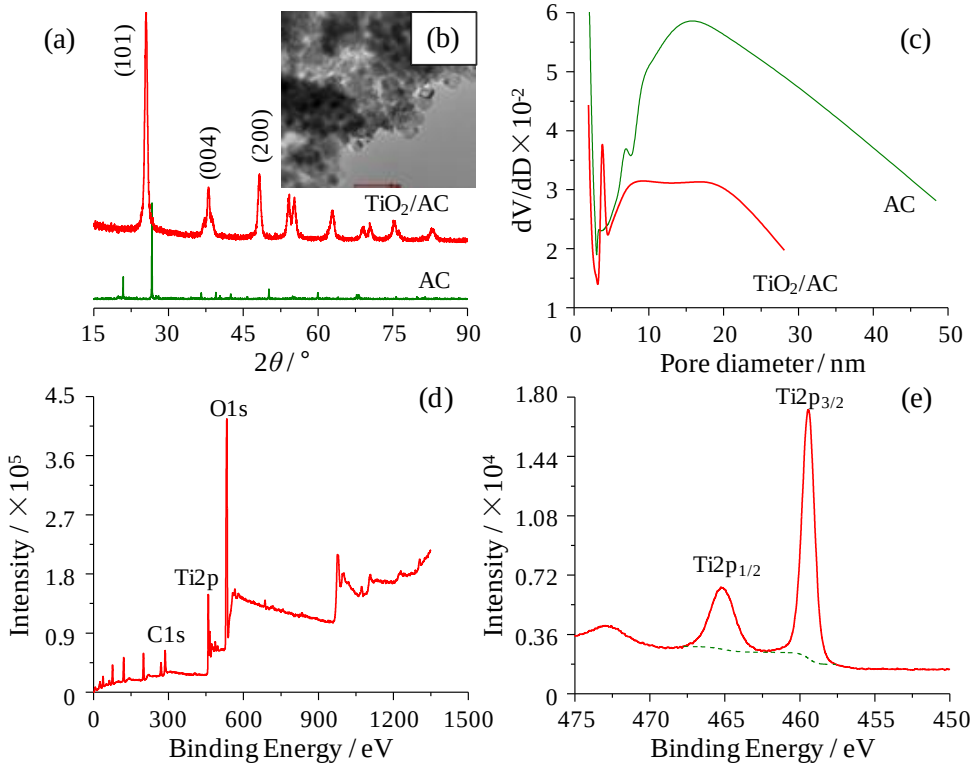


**Figure 1.** The microstructures and component of AC and the prepared $TiO_2$/AC. (a) XRD pattern, (b) TEM image, (c) porosity volume ratio, (d) XPS survey spectra, (e) Ti2p XPS spectra.

While for $TiO_2$/AC, the porosity volume corresponding to the same pore diameter obviously decreases due to the intercalation of active component but the pore structure is approximate to uniform distribution, which is of benefit to efficient diffusion of reactants. In Fig. 1(d), XPS survey spectra illustrates the elements O, Ti and C at binding energies of 532.77 eV, 459.27 eV and 286.82 eV with atomic concentrations of 55.83%, 6.04% and 14.18%, respectively. As shown in Fig. 1(e), the two peaks at about 459.43 eV and 465.28 eV correspond to binding energies of Ti $2p_{3/2}$ and Ti $2p_{1/2}$. The peak at binding energy of 459.43 eV is assigned to $Ti^{4+}$ in $TiO_2$ lattice [14] and it is also found that the FWHM of Ti $2p_{3/2}$ is 0.96 eV, which demonstrates the prepared $TiO_2$ exists in monocrystal state that possesses higher ability for generation of hydroxyl radicals.

The CV curves and EIS spectra of the AC and $TiO_2$/AC coupled with $IrO_2$-$Ta_2O_5$/Ti anode in phenolic solution are provided in Fig. 2. Phenol oxidation peaks on the two electrodes could not be seen from the CV scans. However, obvious *rex-ox* peaks in potentials regions of 1.28-1.45 V and 0.86-1.08 V corresponding to conversion of $IrO_2$ supported on Ti substrate are detected if AC particulate electrode was used. These reactions are associated with the reduction of $IrO_3$ to $IrO_2$ and the oxidation of $IrO_2$ to $IrO_3$, respectively [15,16]. In contrast, slight oxidation peak can be obtained when $TiO_2$/AC was employed, but almost non-distinguished reduction peak is shown, probably due to the restrain of Ir(VI)/Ir(IV) conversion by $TiO_2$. Furthermore, it is observed that the peak and feed currents are increased greatly on the $TiO_2$/AC electrode, asserting that $TiO_2$ should possess high electrocatalytic activity for phenol oxidation. Such enhancement can be interpreted by the passivation of particulate electrodes related to their different polymerized films determined by the pore structures [17,18]. The Nyquist complex plane plots of AC and $TiO_2$/AC electrodes are presented in Fig. 2(b).

**Table 1.** Fitted impedance parameters of the two electrodes

| Sample | $R_s$ ($\Omega$ cm$^2$) | $R_e$ ($\Omega$ cm$^2$) | $R_c$ ($\Omega$ cm$^2$) | $R_{ct}$ ($\Omega$ cm$^2$) | $i_0$ ($\times10^{-6}$ A/cm$^2$) |
|---|---|---|---|---|---|
| AC | 9.13 | 625.90 | 17.59 | 52.58 | 6.11 |
| $TiO_2$/AC | 9.21 | 139.40 | 17.86 | 21.70 | 14.80 |

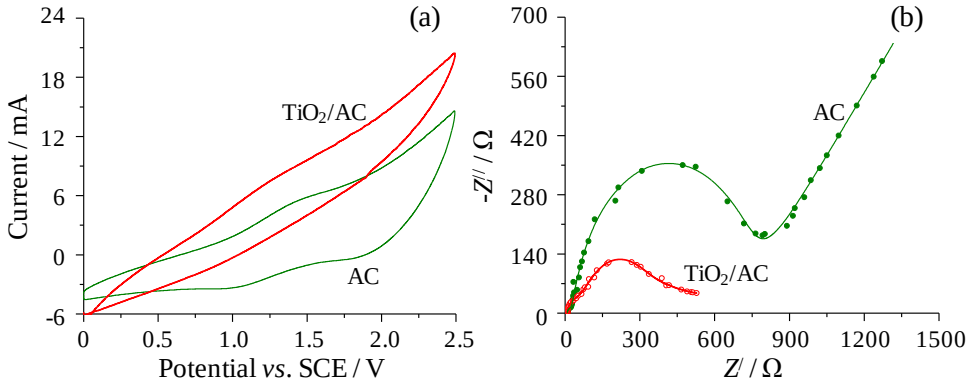


**Figure 2.** CV (a) and EIS (b) curves of AC and $TiO_2$/AC electrodes. The solid curves of EIS represent the simulated ones. In the equivalent circuit, $R_s$ is electrolyte resistance; $R_e$ and $C_e$ are resistance and capacitance of the film on anode; $C_d$ and $Z_w$ are double-layer capacitance and Warburg impedance for electron diffusion.

The less diameter of $TiO_2$/AC illustrates that charge transfer resistance is smaller than that of AC electrode. A Nyquist equivalent circuit of $R_s(CR_e)((CR_c)(Q(R_{ct}W)))$ is employed to simulate the EIS data. Different from other research [19], the resistance of polymerized film on particulate electrode ($R_c$) is introduced to differ the effect of the pore structures, and a constant phase element $Q$ is to describe the impedance behavior of electrodes. The simulated data for the elements are summarized in Table 1. Seen from this table, we observe the $R_c$ values of the two electrodes are almost equal, further confirming the rationality of ignoring their adsorption. After $TiO_2$ intercalation, the anode agglomeration can be retarded and the charge transfer resistance ($R_{ct}$) value is obviously decreased, causing increase of the exchange current density ($i_0$). These results indicate $TiO_2$ could involve in electrooxidation via acting as insulator to separate particulate electrode each other that enhances bipolarity of the AC particles.

Fig. 3 provides a direct comparison of the two electrodes for phenol oxidation. The STY values of $TiO_2$/AC electrode are always higher than those of AC, especially at the initial reaction stage (Fig. 3(a)). The rapid oxidation leads to less power consumption, which is shown in Fig. 3(b), e.g. the values of $E_{sp}$ are 6.3 and 9.1 kWh/kgCOD at reaction time of 52 min when $TiO_2$/AC and AC electrodes are used, respectively, and the former is decreased by ratio of 30.1% to the latter. The UV spectra in Fig. 3(c) directly demonstrate the generation of hydroxyphenol molecules and carboxide or conjugated double bond groups located in 200 nm to 220 nm and 230 nm to 270 nm wavelengths [20,21], respectively. But after analysis of the curves presented in Fig. 3(d), the existence of such complex matters could be excluded, illustrating $TiO_2$/AC could shorten phenol degradation pathway.

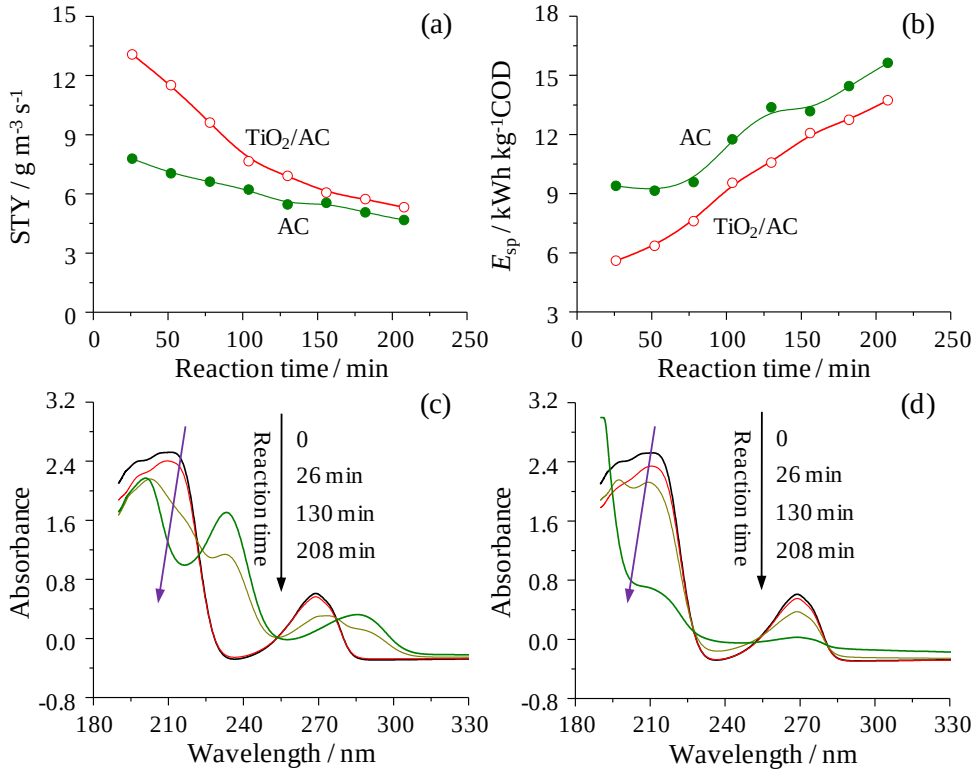


**Figure 3.** The STY (a), power consumption (b) and UV spectrophotometry of samples after phenol oxidation on AC (c) and $TiO_2$/AC (d) electrodes. Experimental conditions: $q$=0.6 L/h, $i$=30 A/m$^2$, $U$=3.8 V, $COD_0$=1383.97 mg/L.

Fig. 4 directly confirms existence of the intermediates, e.g. hydroquinone, benzoquinone and maleic anhydride captured by the GC-MS measurements at the reaction time of 26 min and 208 min with AC electrode; however, except maleic anhydride, there is almost no other intermediate during phenol oxidation on $TiO_2$/AC electrode. Moreover, the accumulation of benzoquinone which is more poisonous than phenol was not found when the $TiO_2$/AC electrode was used. These results depict $TiO_2$ is favorable to accelerate phenol decomposition that could lower power consumption and naturally be considered as a "green" electro-catalyst.

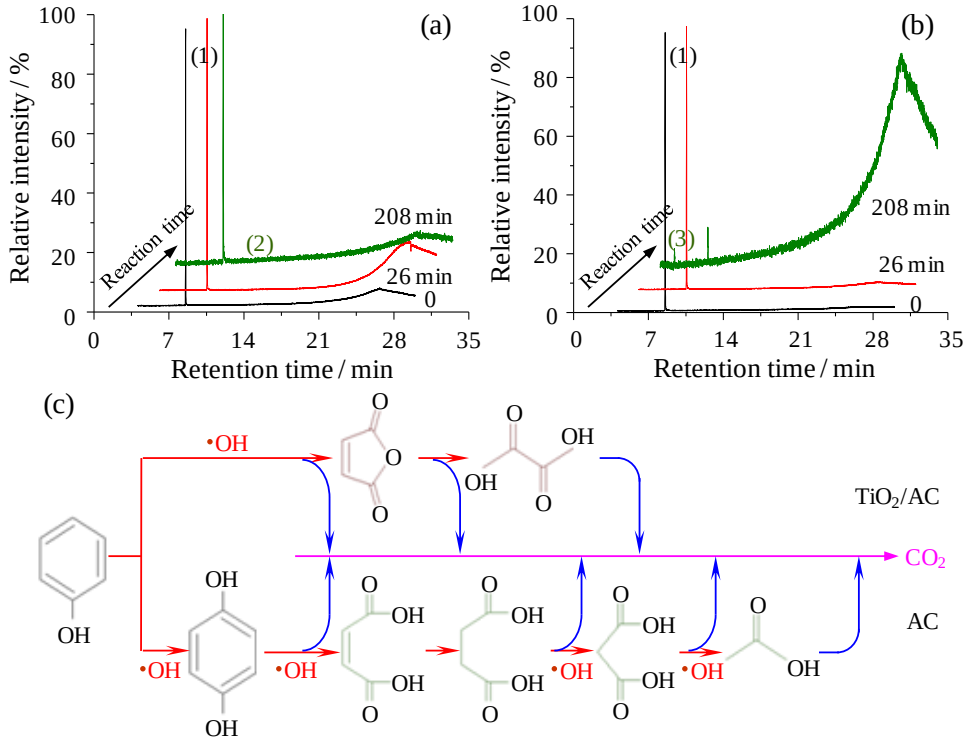


**Figure 4.** GC-MS chromatograms during phenol oxidation on AC (a) and $TiO_2$/AC (b) electrodes, and phenol degradation pathways (c). (1) phenol, (2) benzoquinone, (3) maleic anhydride. Experimental conditions are the same to those shown in Fig. 3.

## 4. CONCLUSION

The prepared nano-$TiO_2$ in anatase type was successfully intercalated in AC micropores. Compared with AC particles, the pore structure of $TiO_2$/AC is approximate to uniform distribution with diameter ranged from 7.0 nm to 20.3 nm and XPS analysis show the $TiO_2$ lattice exists in monocrystal state. The enhancement of feed current and exchange current density obtained through CV and EIS measurements illustrate the higher electrochemical performances of $TiO_2$/AC and $TiO_2$ could be used as an excellent catalyst in electrooxidation. The STY for phenol oxidation is accelerated and the power consumption is obviously decreased by the employment of $TiO_2$/AC as particulate electrode. Furthermore, the UV-vis and GC-MS spectra reflect the prepared electrode could shorten phenol degradation pathway and avoid production of poisonous intermediate.

ACKNOWLEDGEMENTS
This work was financially supported by the Fundamental Research Funds for the Central Universities (2013QNA20).

**References**

1. L. Wang, B. Wu, P. Li, B. Zhang, N. Balasubramanian, Y. Zhao, *Chem. Eng. J.*, 284 (2016) 240.
2. A.I. Masliy, N.P. Poddubny, A.Zh. Medvedev, V.O. Lukyanov, *J. Electroanal. Chem.*, 757 (2015) 128.
3. C. Wang, Y.K. Huang, Q. Zhao, M. Ji, *Chem. Eng. J.*, 243 (2014) 1.
4. J. Han, Z. Liu, K. Guo, B. Wang, X. Zhang, T. Hong, *Appl. Catal. B.*, 163 (2015) 179.
5. W. Kong, B. Wang, H. Ma, L. Gu, *J. Hazard. Mater.*, 137 (2006) 1532.
6. H. Zhao, J. Gao, G. Zhao, J. Fan, Y. Wang, Y. Wang, *Appl. Catal. B.*, 136-137 (2013) 278.
7. M. Ouzzine, A.J. Romero-Anaya, M.A. Lillo-Ródenas, A. Linares-Solano, *Carbon*, 67 (2014) 104.
8. S. Horikoshi, S. Sakamoto, N. Serpone, *Appl. Catal. B.*, 140-141 (2013) 646.
9. X. Guo, D. Li, J. Wan, X. Yu, *Electrochim. Acta*, 180 (2015) 957.
10. H. Song, X. Qiu, F. Li, W. Zhu, L. Chen, *Electrochem. Commun*,. 9 (2007) 1416.
11. P. Li, Y. Zhao, L. Wang, B. Ding, Y. Hu, Q. Yan, *Electrochemistry*, 82 (2014) 1056.
12. L. Wang, Y. Hu, Y. Zhang, P. Li, Y. Zhao, *Sep. Purif. Technol.*, 109 (2013) 18.
13. APHA. *Standard methods for examination of water and wastewater*, 20th ed. Washington DC: APHA; 1998.
14. G.J. Fleming, K. Adib, J.A. Rodriguez, M.A. Barteau, J.M. White, H. Idriss, *Surf. Sci.*, 602 (2008) 2029.
15. P. Lakshmipathiraj, G. Bhaskar Raju, Y. Sakai, Y. Takuma, A. Yamasaki, S. Kato, T. Kojima, *Chem. Eng. J.*, 198-199 (2012) 211.
16. E. Chatzisymeon, A. Dimou, D. Mantzavinos, A. Katsaounis, *J. Hazard. Mater.*, 167 (2009) 268.
17. X.M. Wang, J.M. Hu, J.Q. Zhang, C.N. Cao, *Electrochim. Acta*, 53 (2008) 3386.
18. J.K. Wang, J. Farreli, Environ. *Sci. Technol.*, 38 (2004) 5232.
19. S. Yang, H. Song, X. Chen, *Electrochem. Commun.*, 8 (2006) 137.
20. H.Yu, S.Zhu, X. Yang, X. Wang, H. Sun, M. Huo, *PLoS ONE*, 8 (2013) e66447.
21. M. Friedman, H.S. Jürgens, *J. Agric. Food Chem.*, 48 (2000) 2101.